J|A|C|S
ARTICLES
Published on Web 01/10/2006

Aminoglycoside-Induced Reduction in Nucleotide Mobility at the Ribosomal RNA A-Site as a Potentially Key Determinant of Antibacterial Activity

Malvika Kaul, Christopher M. Barbieri, and Daniel S. Pilch*

Contribution from the Department of Pharmacology, University of Medicine and Dentistry of New Jersey, Robert Wood Johnson Medical School, 675 Hoes Lane, Piscataway, New Jersey 08854-5635

Received September 7, 2005; E-mail: pilchds@umdnj.edu

Abstract: Steady-state and time-resolved fluorescence techniques have been used to characterize the energetics and dynamics associated with the interaction of an *E. coli* 16 S rRNA A-site model oligonucleotide and four aminoglycoside antibiotics that exhibit a broad range of antibacterial activity. The results of these characterizations suggest that aminoglycoside-induced reduction in the mobility of an adenine residue at position 1492 of the rRNA A-site is a more important determinant of antibacterial activity than drug affinity for the A-site. This observation is consistent with a recently proposed model for the mechanism of protein synthesis inhibition by aminoglycosides that invokes a drug-induced alteration in the conformational equilibrium of the rRNA A-site (centered around the conserved adenine residues at positions 1492 and 1493), which, in turn, promotes an enhanced interaction between the rRNA and the minihelix formed by the tRNA anticodon and the mRNA codon, even when the anticodon is noncognate. Regarded as a whole, the results reported here indicate that the rational design of antibiotics that target the 16 S rRNA A-site requires consideration of not only the structure and energetics of the drug−RNA complex but also the dynamics associated with that complex.

Introduction

The aminoglycosides are a class of broad-spectrum antimicrobial agents that exhibit rapid and concentration-dependent bactericidal activities.[1] Their antibacterial properties are attributed to interactions with the 30 S ribosomal subunit and subsequent interference with protein synthesis.[1] Aminoglycosides consist of one or more amino sugars glycosidically linked to an aminocyclitol moiety, with this moiety being 2-deoxystreptamine (2-DOS) in all but a few aminoglycosides. The specific molecular target of 2-DOS aminoglycosides within the 30 S ribosomal subunit is the decoding region A-site of the 16 S rRNA.[2−5]

Recent structural studies have provided key insights into the nature of the complexes formed between 2-DOS aminoglycosides and the 16 S rRNA A-site. NMR studies by Puglisi and co-workers on an *E. coli* 16 S rRNA A-site model oligonucleotide and its complexes with paromomycin and gentamicin C1a revealed that the binding of the drugs induced the displacement of two conserved adenine residues at positions 1492 and 1493 (A1492 and A1493) from an intrahelical to an extrahelical state.[6−8] A seminal crystallographic study by Ramakrishnan and co-workers provided the first structure of an intact bacterial 30 S ribosomal subunit in complex with a 2-DOS aminoglycoside (paromomycin).[5] This structure was consistent with the corresponding NMR-derived structure with respect to the binding site and the extrahelical nature of the conformations adopted by A1492 and A1493. One noteworthy difference between the two structures is that the extent to which A1492 and A1493 are positioned away from the helix is greater in the crystal structure than in the NMR-derived structure. Subsequent crystallographic studies by the Westhof[9−11] and Hermann[12,13] groups on the complexes formed between various A-site model

(1) Chambers, H. F. Aminoglycosides and Spectinomycin. In *Basic and Clinical Pharmacology*, 9th ed.; Katzung, B. G., Ed.; McGraw-Hill: New York, 2004; pp 764−772.
(2) Moazed, D.; Noller, H. F. Interaction of Antibiotics with Functional Sites in 16 S Ribosomal RNA. *Nature* **1987**, *327*, 389−394.
(3) De Stasio, E. A.; Moazed, D.; Noller, H. F.; Dahlberg, A. E. Mutations in 16 S Ribosomal RNA Disrupt Antibiotic−RNA Interactions. *EMBO J.* **1989**, *8*, 1213−1216.
(4) Woodcock, J.; Moazed, D.; Cannon, M.; Davies, J.; Noller, H. F. Interaction of Antibiotics with A- and P-Site-Specific Bases in 16 S Ribosomal RNA. *EMBO J.* **1991**, *10*, 3099−3103.
(5) Carter, A. P.; Clemons, W. M.; Brodersen, D. E.; Morgan-Warren, R. J.; Wimberly, B. T.; Ramakrishnan, V. Functional Insights from the Structure of the 30 S Ribosomal Subunit and its Interactions with Antibiotics. *Nature* **2000**, *407*, 340−348.
(6) Fourmy, D.; Recht, M. I.; Blanchard, S. C.; Puglisi, J. D. Structure of the A Site of *Escherichia coli* 16 S Ribosomal RNA Complexed with an Aminoglycoside Antibiotic. *Science* **1996**, *274*, 1367−1371.
(7) Fourmy, D.; Yoshizawa, S.; Puglisi, J. D. Paromomycin Binding Induces a Local Conformational Change in the A-Site of 16 S rRNA. *J. Mol. Biol.* **1998**, *277*, 333−345.
(8) Yoshizawa, S.; Fourmy, D.; Puglisi, J. D. Structural Origins of Gentamicin Antibiotic Action. *EMBO J.* **1998**, *17*, 6437−6448.
(9) Vicens, Q.; Westhof, E. Crystal Structure of Paromomycin Docked into the Eubacterial Ribosomal Decoding A Site. *Structure* **2001**, *9*, 647−658.
(10) Vicens, Q.; Westhof, E. Crystal Structure of a Complex between the Aminoglycoside Tobramycin and an Oligonucleotide Containing the Ribosomal Decoding A Site. *Chem. Biol.* **2002**, *9*, 747−755.
(11) Vicens, Q.; Westhof, E. Crystal Structure of Geneticin Bound to a Bacterial 16 S Ribosomal RNA A Site Oligonucleotide. *J. Mol. Biol.* **2003**, *326*, 1175−1188.

oligonucleotide constructs and a number of different 2-DOS aminoglycosides revealed extrahelical conformations for A1492 and A1493 that were similar to those in the complex of the 30 S ribosomal subunit with paromomycin. The crystallographic studies conducted by Hermann and co-workers also included characterizations of the drug-free A-site model oligonucleotide constructs.[12,13] Significantly, these studies demonstrated that A1492 and A1493 can adopt extrahelical conformations even in the absence of bound drug.

An important set of mutational studies by Yoshizawa et al.[14] provided the first indication that the ribosome may recognize the mRNA codon−tRNA anticodon complex through interactions with A1492 and A1493 of the 16 S rRNA. The detailed nature of these interactions were then elegantly delineated by Ogle et al.[15] in their reported crystal structure of a bacterial 30 S ribosomal subunit in ternary complex with an mRNA codon and an aminoacyl tRNA anticodon. In this structure, A1492 and A1493 adopt extrahelical conformations, which, in turn, enable these bases to engage in a series of contacts with the minor groove of the minihelix formed by the mRNA codon and tRNA anticodon. Aminoglycoside-induced modulation of such contacts may explain the results of kinetic studies by Karimi and Ehrenberg,[16] which demonstrated that neomycin reduced the rate at which aminoacyl−tRNA dissociates from the A-site of ribosomes by approximately 6-fold at 37 °C.

2-DOS aminoglycoside targeting of the 16 S rRNA A-site interferes with the translation of mRNA in three ways: (i) inhibition of initiation, (ii) mistranslation (incorporation of incorrect amino acids into the growing polypeptide chain), and (iii) premature termination (via inhibition of the translocation step).[1,17] The structural and biochemical studies described above have provided crucial insights into the potential mechanism by which aminoglycosides exert their deleterious effects on protein synthesis. These insights have resulted in a proposed mechanism that is based on the premise that A1492 and A1493 of the 16 S rRNA play an important role in maintaining translational fidelity. The proposed mechanism (schematically depicted in Figure 1) postulates that A1492 and A1493 are in conformational equilibria between intrahelical and extrahelical states. In their extrahelical states, A1492 and A1493 are able to interact with the codon−anticodon minihelix, with this interaction being favored in the presence of the cognate tRNA anticodon and disfavored in the presence of a noncognate tRNA anticodon (see Figure 1A). The binding of a 2-DOS aminoglycoside shifts the conformational equilibria of A1492 and A1493 toward the extrahelical state, thereby resulting in an enhanced interaction with the codon−anticodon minihelix, even when the anticodon is noncognate (see Figure 1B). Consistent with this model, we have previously shown that binding-induced destacking of the base at position 1492 is an important factor in dictating the prokaryotic specificity of aminoglycoside action.[18] The studies described herein are designed to further explore the veracity of the proposed model. To this end, we used both steady-state and time-resolved fluorescence techniques to compare and contrast the binding of four aminoglycosides (see structures in Figure 2) that exhibit a range of bactericidal activities to an oligonucleotide construct that has been shown to be an effective model of the *E. coli* 16 S rRNA A-site.[19,20] The adenine at position 1492 in this A-site model oligomer (hereafter designated as Ec2AP1492) was substituted with the fluorescent base analogue 2-aminopurine (2AP), with the sequence and secondary structure of Ec2AP1492 being depicted in Figure 3. Our collective results suggest that the extent of aminoglycoside-induced reduction in the mobility of the base at position 1492 is a more important determinant of antibacterial potency than either the observed extent to which drug binding destacks the 1492 base or the magnitude of drug affinity for the rRNA A-site.

Materials and Methods

RNA and Drug Molecules. Ec2AP1492 was obtained in its PAGE-purified sodium salt form from Dharmacon Research, Inc. (Lafayette, CO). The concentrations of all Ec2AP1492 solutions were determined spectrophotometrically using an extinction coefficient at 260 nm and 85 °C of 248 370 ± 940 (mol strand/L)$^{-1}$·cm^{-1}. This extinction coefficient was determined by enzymatic digestion and subsequent colorimetric phosphate assay using previously established protocols.[21] Paromomycin·H_2SO_4, neomycin·$3H_2SO_4$·$3H_2O$, and geneticin (G418)·$2H_2SO_4$ were obtained from Fluka, while ribostamycin·$2.5H_2SO_4$ was obtained from Sigma. All drugs were used without further purification.

Antibacterial Assay. *E. coli* DH5α cells in log phase were grown at 37 °C in Luria-Bertani (LB) medium containing 2-fold serial dilutions of neomycin, paromomycin, ribostamycin, or G418 to yield final concentrations ranging from 200 μM to 10 nM. Bacterial growth was monitored after 24 h by measuring optical density at 620 nm, with the minimum inhibitory concentration (MIC) being defined as the lowest drug concentration at which growth is completely inhibited. Antibacterial activities were assayed in at least three independent experiments, with each experiment including three replicates of each drug concentration.

Steady-State Fluorescence Spectroscopy. All steady-state fluorescence experiments were conducted at 25 °C on an AVIV model ATF105 spectrofluorometer (AVIV Biomedical; Lakewood, NJ) equipped with a thermoelectrically controlled cell holder. The excitation wavelength was set at 310 nm in all the experiments, with the excitation and emission slit widths being set at 3 and 4 nm, respectively. A quartz cell with a 1 cm path length in both the excitation and emission directions was used for all measurements unless noted otherwise.

(12) Shandrick, S.; Zhao, Q.; Han, Q.; Ayida, B. K.; Takahashi, M.; Winters, G. C.; Simonsen, K. B.; Vourloumis, D.; Hermann, T. Monitoring the Molecular Recognition of the Ribosomal Decoding Site. *Angew. Chem., Int. Ed.* **2004**, *43*, 3177−3182.
(13) Zhao, F.; Zhao, Q.; Blount, K. F.; Han, Q.; Tor, Y.; Hermann, T. Molecular Recognition of RNA by Neomycin and a Restricted Neomycin Derivative. *Angew. Chem., Int. Ed.* **2005**, *44*, 5329−5334.
(14) Yoshizawa, S.; Fourmy, D.; Puglisi, J. D. Recognition of the Codon−Anticodon Helix by Ribosomal RNA. *Science* **1999**, *285*, 1722−1725.
(15) Ogle, J. M.; Brodersen, D. E.; Clemons, W. M., Jr.; Tarry, M. J.; Carter, A. P.; Ramakrishnan, V. Recognition of Cognate Transfer RNA by the 30*S* Ribosomal Subunit. *Science* **2001**, *292*, 897−902.
(16) Karimi, R.; Ehrenberg, M. Dissociation Rate of Cognate Peptidyl−tRNA from the A-Site of Hyper-Accurate and Error-Prone Ribosomes. *Eur. J. Biochem.* **1994**, *226*, 355−360.
(17) Puglisi, J. D.; Blanchard, S. C.; Dahlquist, K. D.; Eason, R. G.; Fourmy, D.; Lynch, S. R.; Recht, M. I.; Yoshizawa, S. Aminoglycoside Antibiotics and Decoding. In *The Ribosome: Structure, Function, Antibiotics, and Cellular Interactions*; Garrett, R. A., Douthwaite, S. R., Liljas, A., Matheson, A. T., Moore, P. B., Noller, H. F., Eds.; ASM Press: Washington, DC, 2000; pp 419−429.
(18) Kaul, M.; Barbieri, C. M.; Pilch, D. S. Defining the Basis for the Specificity of Aminoglycoside−rRNA Recognition: A Comparative Study of Drug Binding to the A Sites of *Escherichia coli* and Human rRNA. *J. Mol. Biol.* **2005**, *346*, 119−134.
(19) Recht, M. I.; Fourmy, D.; Blanchard, S. C.; Dahlquist, K. D.; Puglisi, J. D. RNA Sequence Determinants for Aminoglycoside Binding to an A-Site rRNA Model Oligonucleotide. *J. Mol. Biol.* **1996**, *262*, 421−436.
(20) Miyaguchi, H.; Narita, H.; Sakamoto, K.; Yokoyama, S. An Antibiotic-Binding Motif of an RNA Fragment Derived from the A-Site-Related Region of *Escherichia coli* 16S rRNA. *Nucleic Acids Res.* **1996**, *24*, 3700−3706.
(21) Plum, G. E. Optical Methods. In *Current Protocols in Nucleic Acid Chemistry*; Beaucage, S. L., Bergstrom, D. E., Glick, G. D., Jones, R. A., Eds.; John Wiley & Sons: New York, 2000; Vol. 1, pp 7.3.1−7.3.17.

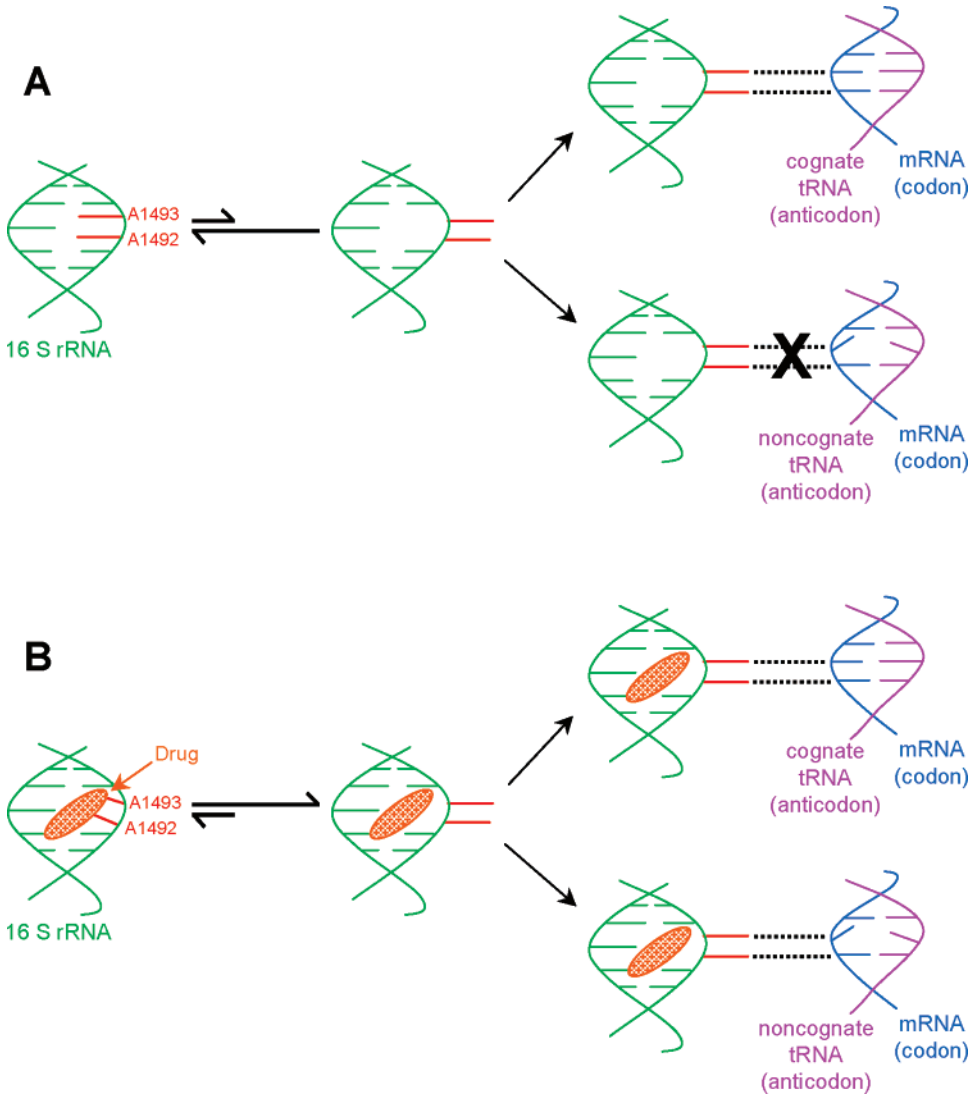

Figure 1. (A) Schematic representation of the proposed role that the adenine residues at positions 1492 and 1493 (denoted as A1492 and A1493 and depicted in red) of the 16 S rRNA (depicted in green) play in maintaining translational fidelity. A1492 and A1493 are in conformational equilibria between intrahelical and extrahelical states, with the intrahelical states being favored in the absence of drug. In their extrahelical states, A1492 and A1493 are able to interact with the minor groove of the minihelix formed by the tRNA anticodon (depicted in magenta) and the mRNA codon (depicted in blue), with this interaction being favored in the presence of the cognate tRNA anticodon and disfavored in the presence of a noncognate tRNA anticodon. (B) Schematic representation of how aminoglycoside binding to the 16 S rRNA affects the mechanism described in (A). The drug (depicted in brown) binds to the 16 S rRNA and shifts the conformational equilibria of A1492 and A1493 toward their extrahelical states. As a result of this drug-induced alteration in the conformational equilibrium of the 16 S rRNA, A1492 and A1493 are now able to engage in favorable interactions with the codon−anticodon minihelix, even when the anticodon is noncognate.

For the fluorescence titration experiments, 1.2−20 μL aliquots of drug (at concentrations ranging from 250 μM to 10 mM) were sequentially added to Ec2AP1492 solutions that were 1 μM in strand. After each addition, the sample was left to equilibrate for 3 min, whereupon the average emission intensity at 370 nm (I_{370}) over a period of 30 s was recorded. Solution conditions were 10 mM EPPS (pH 7.5), 0.1 mM EDTA, and sufficient NaCl to bring the total Na^+ concentration to 100 mM. The I_{370} values of all samples were corrected by subtraction of the corresponding values of buffer alone.

Fluorescence quantum yield values (Φ) of Ec2AP1492 and its complexes with neomycin, paromomycin, ribostamycin, and G418 were determined relative to quinine sulfate in 1 N H_2SO_4, which was assigned a value of 0.546 at 25 °C.[22] For these determinations, the Ec2AP1492 concentration was 18 μM in strand, while the concentration of quinine sulfate was 24 μM. When present, the drug concentrations were chosen so as to ensure that all the Ec2AP1492 was drug-bound under the solution conditions employed. These drug concentrations were as follows: [neomycin] = 90 μM, [paromomycin] = 90 μM, [ribostamycin] = 7.2 mM, and [G418] = 1.8 mM. Fluorescence emission spectra were acquired from 605 to 320 nm in 1 nm increments. All fluorescence emission spectra were corrected by subtraction of the corresponding spectrum of buffer alone. In these measurements, the path lengths of the quartz cell were 0.2 cm in the excitation direction and 1 cm in the emission direction. Solution conditions for the quantum yield experiments were identical to those described above for the fluorescence titration experiments.

Time-Resolved Fluorescence Spectroscopy. Time-resolved fluorescence experiments were conducted at 25 °C on a PTI LaserStrobe fluorescence lifetime spectrometer equipped with a thermoelectrically controlled cell holder. A PTI Model GL-3300 nitrogen laser (at a 10 Hz frequency) was used to excite the samples at 337 nm, and the fluorescence decay curves were acquired logarithmically at an emission wavelength of 400 nm (slit widths ranging from 5 to 8 nm) in 400

(22) Szabo, A. G. Fluorescence Principles and Measurement. In *Spectrophotometry & Spectrofluorimetry*; Gore, M. G., Ed.; Oxford University Press: New York, 2000; pp 33−67.

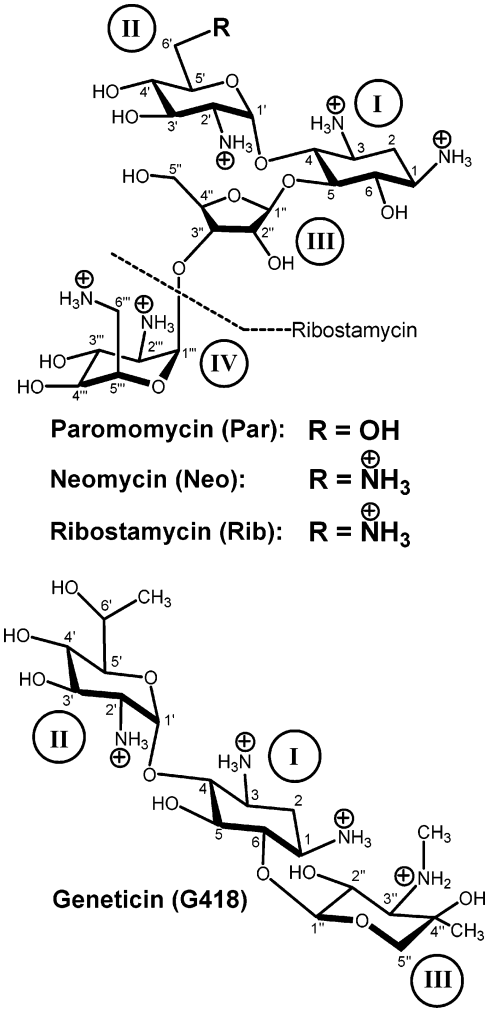

Figure 2. Structures of the four aminoglycosides studied here in their fully protonated cationic states, with the atomic and ring numbering systems denoted in Arabic and Roman numerals, respectively. Ring I in each structure is the aminocyclitol moiety 2-deoxystreptamine (2-DOS). Unlike neomycin and paromomycin, ribostamycin lacks ring IV (as indicated by the dashed line).

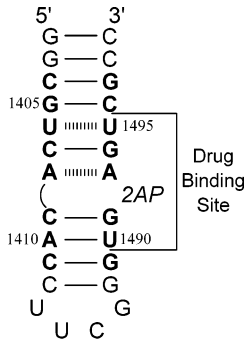

Figure 3. Secondary structure of the *E. coli* 16 S rRNA A-site model oligonucleotide, Ec2AP1492. Bases present in *E. coli* 16 S rRNA are depicted in bold face and are numbered as they are in 16 S rRNA. The 2-aminopurine residue at position 1492 is denoted by *2AP*. The drug binding site (as revealed by footprinting, NMR, and crystallographic studies[6,9,11,19]) is indicated.

channels (with 5 laser shots per time point). The start and end delays of the acquisitions were 37 and 75 ns, respectively. The instrument response function was detected at 337 nm using light scattered by a dilute suspension of nondairy creamer. Each final decay profile reflected an average of 10 independent scans and was deconvolved in the Felix32 program (PTI, Inc.). Goodness of fit was judged based on a reduction in χ^2 and inspection of the autocorrelation function of the weighted residuals. The RNA concentration was 2 μM in strand, and, when present, RNA-saturating concentrations of drug were used. These drug concentrations were as follows: [neomycin] = 10 μM, [paromomycin] = 60 μM, [ribostamycin] = 800 μM, and [G418] = 1.8 mM. Solution conditions for these experiments were identical to those described above for the fluorescence titration experiments. Fluorescence intensity decays were best fit by the following sum of three exponentials:

$$I(t) = \sum_{i=1}^{3} \alpha_i e^{-t/\tau_i} \tag{1}$$

In this relationship, the values of α_i are the amplitudes of each component, and the values of τ_i are the corresponding fluorescence lifetimes. Increasing the number of exponentials above 3 did not result in appreciably improved fits of the decay data. Amplitude-weighted lifetimes ($\bar{\tau}$) were calculated using the following relationship:

$$\bar{\tau} = \frac{\sum_{i=1}^{3} \alpha_i \tau_i}{\sum_{i=1}^{3} \alpha_i} \tag{2}$$

Time-resolved anisotropy measurements were conducted at 25 °C using a sheet polarizer in the emission direction and a Glan-Thompson-type polarizer in the excitation direction. The samples were excited at 337 nm, and the fluorescence decay curves were acquired logarithmically at an emission wavelength of 410 nm (24 nm slit width) in 400 channels (with 5 laser shots per time point). The start and end delays of the acquisitions were identical to those described above, with each final decay profile reflecting an average of 10 independent scans. The RNA concentration was 5 μM in strand, and, when present, RNA-saturating concentrations of drug were employed. These drug concentrations were as follows: [neomycin] = 20 μM, [paromomycin] = 40 μM, [ribostamycin] = 500 μM, and [G418] = 1.8 mM. Solution conditions for these experiments were identical to those described above for the fluorescence titration experiments. Fluorescence intensity decays measured with the emission polarizer oriented either parallel $\{I_{VV}(t)\}$ or perpendicular $\{I_{VH}(t)\}$ to the excitation polarization were deconvolved simultaneously with a magic angle decay $\{D(t)\}$ using the following relationships:

$$I_{VV}(t) = \frac{D(t)[1 + 2r(t)]}{3} \tag{3a}$$

$$I_{VH}(t) = \frac{D(t)[1 - r(t)]}{3G} \tag{3b}$$

In these relationships, G is the instrumental correction factor and $r(t)$ is the anisotropy decay, which was best fit by the following sum of two exponentials:

$$r(t) = \beta_1 e^{-t/\phi_1} + \beta_2 e^{-t/\phi_2} \tag{4}$$

The limiting anisotropy at time zero $\{r(0)\}$ was derived from the sum of β_1 and β_2. Values of G ranged from 1.07 to 1.11 and were determined using the following relationship:

$$G = \frac{\int I_{HV}(t)\mathrm{d}t}{\int I_{HH}(t)\mathrm{d}t} \tag{5}$$

Table 1. Antibacterial Activities and Ec2AP1492 Binding Affinities of Ribostamycin, Paromomycin, G418, and Neomycin

drug	MIC (μM)[a]	K_a (M^{-1})[b]
ribostamycin	25.0	$(1.2 \pm 0.1) \times 10^5$
paromomycin	12.5	$(2.1 \pm 0.3) \times 10^6$
G418	6.3	$(5.4 \pm 0.4) \times 10^4$
neomycin	3.1	$(3.0 \pm 0.5) \times 10^7$

[a] Antibacterial activities versus *E. coli* DH5α cells were assayed in at least three independent experiments. For each drug, the MIC (minimal inhibitory concentration) value obtained was identical in each of the experiments. Consequently, the indicated MIC values reflect averages over at least three independent experiments, with the standard deviations from the mean being zero. [b] Values of K_a were derived from fits of the fluorescence titration data shown in Figure 4 with eq 6. The indicated uncertainties reflect the 95% confidence intervals.

Computational Derivation of Harmonic Mean Correlation Times for Ec2AP1492. Harmonic mean correlation times for the NMR-derived structure of an RNA hairpin 27mer (PDB code 1a3m)[7] identical to Ec2AP1492, with the exception of having an adenine at position 1492 instead of a 2AP residue, were calculated as a function of atomic hydrodynamic radius (a) using the HYDROPRO version 5a software suite.[23,24] In these calculations, the temperature, solvent viscosity, and solvent density were set to 298.15 K, 0.0089 poise, and 1.000 g/cm^3, respectively, with values of a ranging from 1.5 to 6.0 Å. At each value of a, six shell models were generated ($N_\sigma = 6$). Each shell model contained minibeads of a specific radius (σ), with this radius differing in the different models. Minimum and maximum values of σ were selected so as to ensure that the number of minibeads in each shell model fell within the range of 200−2000.

Results and Discussion

The Relative Affinities of 2-DOS Aminoglycosides for the 16 S rRNA A-Site Do Not Correlate with Their Relative Antibacterial Activities. We compared the bactericidal potencies of neomycin, paromomycin, ribostamycin, and G418 versus *E. coli* DH5α bacteria. The minimum inhibitory concentrations (MICs) at which no bacterial growth was observed are summarized in Table 1. Inspection of these MIC data reveals that the four drugs exhibit the following hierarchy of bactericidal activity: neomycin (MIC = 3.1 μM) > G418 (MIC = 6.3 μM) > paromomycin (MIC = 12.5 μM) > ribostamycin (MIC = 25.0 μM). Recall that the antibacterial activities of 2-DOS aminoglycosides are ascribed to their specific recognition of the 16 S rRNA A-site and subsequent interference with protein synthesis. We therefore sought to evaluate the relationship, if any, between aminoglycoside affinity for the rRNA A-site and antibacterial activity. To this end, we compared the affinities of the four drugs for Ec2AP1492. We determined drug−RNA association constants (K_a) by analyzing the drug-induced changes in the fluorescence of Ec2AP1492 with the following formalism:

$$I = I_0 + \frac{(I_\infty - I_0)}{2}\left[\left([\mathrm{D}]_{tot} + [\mathrm{R}]_{tot} + \frac{1}{K_a}\right) - \sqrt{\left([\mathrm{D}]_{tot} + [\mathrm{R}]_{tot} + \frac{1}{K_a}\right)^2 - 4[\mathrm{D}]_{tot}[\mathrm{R}]_{tot}}\right] \quad (6)$$

In this relationship, I_0 and I are the fluorescence emission intensity of the RNA in the absence and presence of drug, respectively; I_∞ is the fluorescence emission intensity of the RNA in the presence of an infinite drug concentration, and $[\mathrm{D}]_{tot}$ and $[\mathrm{R}]_{tot}$ are the total concentrations of drug and RNA, respectively.

Figure 4 shows the fluorescence titrations of Ec2AP1492 with ribostamycin (A), paromomycin (B), G418 (C), and neomycin (D) at pH 7.5 and a Na^+ concentration of 100 mM. Note that the binding of each drug increases the fluorescence intensity of the host duplex, with the fractional change in intensity per increase in drug concentration being the greatest for neomycin and the least for G418. The drug−RNA K_a values derived from fits of these titrations with eq 6 are listed in Table 1. Inspection of these K_a values reveals the following hierarchy of binding affinity: neomycin $\{K_a = (3.0 \pm 0.5) \times 10^7\ M^{-1}\}$ > paromomycin $\{K_a = (2.1 \pm 0.3) \times 10^6\ M^{-1}\}$ > ribostamycin $\{K_a = (1.2 \pm 0.1) \times 10^5\ M^{-1}\}$ > G418 $\{K_a = (5.4 \pm 0.4) \times 10^4\ M^{-1}\}$. Note the lack of concordance between this hierarchy of RNA binding affinity and the corresponding hierarchy of antibacterial activity noted above. As an illustrative example, the antibacterial potency of G418 is 2-fold greater than that of paromomycin, yet its affinity for the rRNA A-site is 39-fold lower. Taken together, these observations suggest that affinity for the rRNA A-site is not the sole, or perhaps even the most important, determinant of antibacterial activity. In support of this hypothesis, Wong and co-workers have shown that 2-DOS aminoglycosides with antibacterial potencies that are known to be similar exhibit differing specificities for the 16 S rRNA A-site.[25,26]

Not Only Does Antibacterial Potency Fail to Correlate with Affinity for the 16 S rRNA A-Site, but it Also Fails to Correlate with the Observed Extent of Drug-Induced Destacking of the Base at Position 1492. Recall that the drug-induced destacking of the adenine residues at positions 1492 and 1493 of the 16 S rRNA A-site is thought to play an important role in the inhibitory effects that the aminoglycosides exert on protein synthesis.[5−7,9,14,15,17] We sought to determine whether the relative antibacterial activities of neomycin, paromomycin, ribostamycin, and G418 correlate with the observed extents to which the RNA binding of these drugs induces the destacking of the base at position 1492. Specifically, we used a combination of steady-state and time-resolved fluorescence measurements to quantify the apparent extents to which the binding of the four drugs to Ec2AP1492 induces destacking of the 2AP residue. The extent of drug-induced base destacking can be determined from fluorescence quantum yield (Φ) and lifetime (τ) information by calculating the fraction of stacked base ($f_{stacked}$) using the following relationship:[27]

$$f_{stacked} = 1 - \Phi_{rel}/\bar{\tau}_{rel} \quad (7)$$

In this relationship, Φ_{rel} ($=\Phi/\Phi_{r2AP}$) and $\bar{\tau}_{rel}$ ($=\bar{\tau}/\bar{\tau}_{r2AP}$) are the quantum yield and amplitude-weighted fluorescence lifetime of

(23) García de la Torre, J.; Huertas, M. L.; Carrasco, B. Calculation of Hydrodynamic Properties of Globular Proteins from Their Atomic-Level Structure. *Biophys. J.* **2000**, *78*, 719−730.
(24) Fernandes, M. X.; Ortega, A.; López Martínez, M. C.; García de la Torre, J. Calculation of Hydrodynamic Properties of Small Nucleic Acids from Their Atomic Structure. *Nucleic Acids Res.* **2002**, *30*, 1782−1788.
(25) Alper, P. B.; Hendrix, M.; Sears, P.; Wong, C.-H. Probing the Specificity of Aminoglycoside−Ribosomal RNA Interactions with Designed Synthetic Analogs. *J. Am. Chem. Soc.* **1998**, *120*, 1965−1978.
(26) Wong, C.-H.; Hendrix, M.; Priestley, E. S.; Greenberg, W. A. Specificity of Aminoglycoside Antibiotics for the A-Site of the Decoding Region of Ribosomal RNA. *Chem. Biol.* **1998**, *5*, 397−406.
(27) Rachofsky, E. L.; Seibert, E.; Stivers, J. T.; Osman, R.; Ross, J. B. A. Conformation and Dynamics of Abasic Sites in DNA Investigated by Time-Resolved Fluorescence of 2-Aminopurine. *Biochemistry* **2001**, *40*, 957−967.

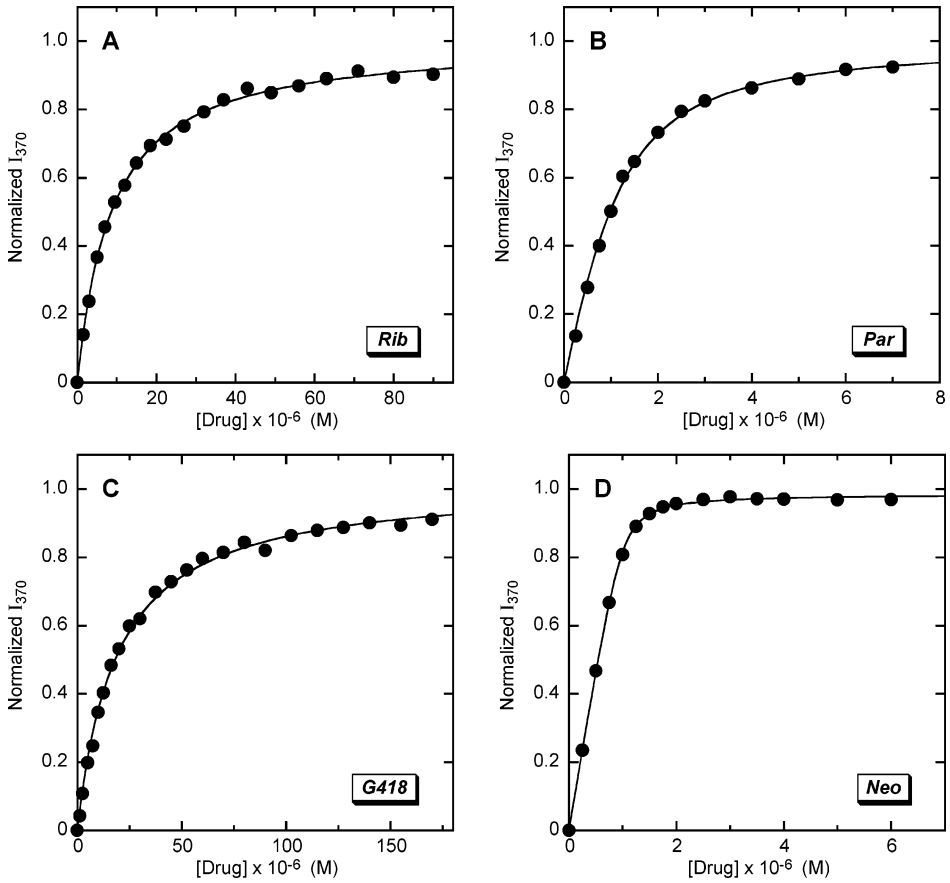

Figure 4. Fluorescence profiles for the titration of (A) ribostamycin (Rib), (B) paromomycin (Par), (C) G418, and (D) neomycin (Neo) into a solution of Ec2AP1492 at 25 °C. The solid lines represent the fits of the experimental data with eq 6. The RNA concentration was 1 μM in strand, and the solution conditions were 10 mM EPPS (pH 7.5), 0.1 mM EDTA, and sufficient NaCl to bring the total Na^+ concentration to 100 mM. For clarity of presentation, the fluorescence intensity at 370 nm (I_{370}) was normalized by dividing the observed change in I_{370} ($I_{370} - I_0$) by the total calculated change in I_{370} ($I_\infty - I_0$).

2AP in the RNA or drug−RNA complex relative to the corresponding fluorescence parameters of the free riboside (r2AP). Barkley and co-workers have previously reported Φ and $\bar{\tau}$ values for r2AP of 0.74 and 10.7 ns, respectively.[28] By definition, the value of $f_{stacked}$ for r2AP is 0.

We analyzed the steady-state fluorescence intensities of Ec2AP1492 and its complexes with the four drugs to yield the Φ values listed in Table 2. Note that drug binding increases the Φ value of Ec2AP1492, with the extent of this increase being greater for paromomycin ($\Delta\Phi = 0.079$) and G418 ($\Delta\Phi = 0.034$) than for neomycin ($\Delta\Phi = 0.018$) and ribostamycin ($\Delta\Phi = 0.010$). We complemented our steady-state fluorescence characterizations with time-resolved fluorescence studies of Ec2AP1492 and its complexes with the four drugs. A representative set of fluorescence intensity decays that emerged from these studies is shown in Figure 5. Global analyses (as described in the Materials and Methods) of these decays, as well as a corresponding decay of drug-free Ec2AP1492, yielded the decay parameters (τ_i and α_i) listed in Table 3. All the decays were best described by the sum of three exponential terms (eq 1), with the number of lifetimes and their magnitudes being similar to those previously reported by us and others for various 2AP-substituted RNA and DNA duplexes.[18,27−29]

Table 2. Steady-State and Time-Resolved Fluorescence Parameters for Ec2AP1492 and its Complexes with Ribostamycin (Rib), Paromomycin (Par), G418, and Neomycin (Neo) at 25 °C

sample	Φ (±0.001)	$\bar{\tau}^b$ (ns)	$f_{stacked}$ [c]
r2AP	0.74[a]	10.7[a]	0
Ec2AP1492	0.027	1.25 ± 0.15	0.69 ± 0.04
Ec2AP1492−Rib	0.037	1.26 ± 0.16	0.58 ± 0.07
Ec2AP1492−Par	0.106	2.51 ± 0.09	0.39 ± 0.03
Ec2AP1492- G418	0.061	1.76 ± 0.10	0.50 ± 0.03
Ec2AP1492− Neo	0.045	1.65 ± 0.05	0.60 ± 0.02

[a] Values of Φ and $\bar{\tau}$ for r2AP were taken from Tsujikawa et al.[28] [b] The values of $\bar{\tau}$ (calculated using eq 2) represent averages of at least two independent experiments, with the indicated uncertainties reflecting the standard deviations from the mean. [c] Values of $f_{stacked}$ were calculated using eq 7, with the indicated uncertainties reflecting the maximum possible errors as propagated through this equation. The value of $f_{stacked}$ for r2AP is zero by definition.

We used the decay parameters listed in Table 3, as well as the corresponding parameters derived from a second independent set of experiments (not shown), to calculate (using eq 2) the $\bar{\tau}$ values listed in Table 2. These $\bar{\tau}$ values, coupled with the corresponding values of Φ, enabled us to determine values of $f_{stacked}$ using eq 7. Inspection of these $f_{stacked}$ values, which are listed in Table 2, reveals the following significant features:

(28) Tsujikawa, L.; Strainic, M. G.; Watrob, H.; Barkley, M. D.; deHaseth, P. L. RNA Polymerase Alters the Mobility of an A-Residue Crucial to Polymerase-Induced Melting of Promoter DNA. *Biochemistry* **2002**, *41*, 15334−15341.

(29) Kaul, M.; Barbieri, C. M.; Pilch, D. S. Fluorescence-Based Approach for Detecting and Characterizing Antibiotic-Induced Conformational Changes in Ribosomal RNA: Comparing Aminoglycoside Binding to Prokaryotic and Eukaryotic Ribosomal RNA Sequences. *J. Am. Chem. Soc.* **2004**, *126*, 3447−3453.

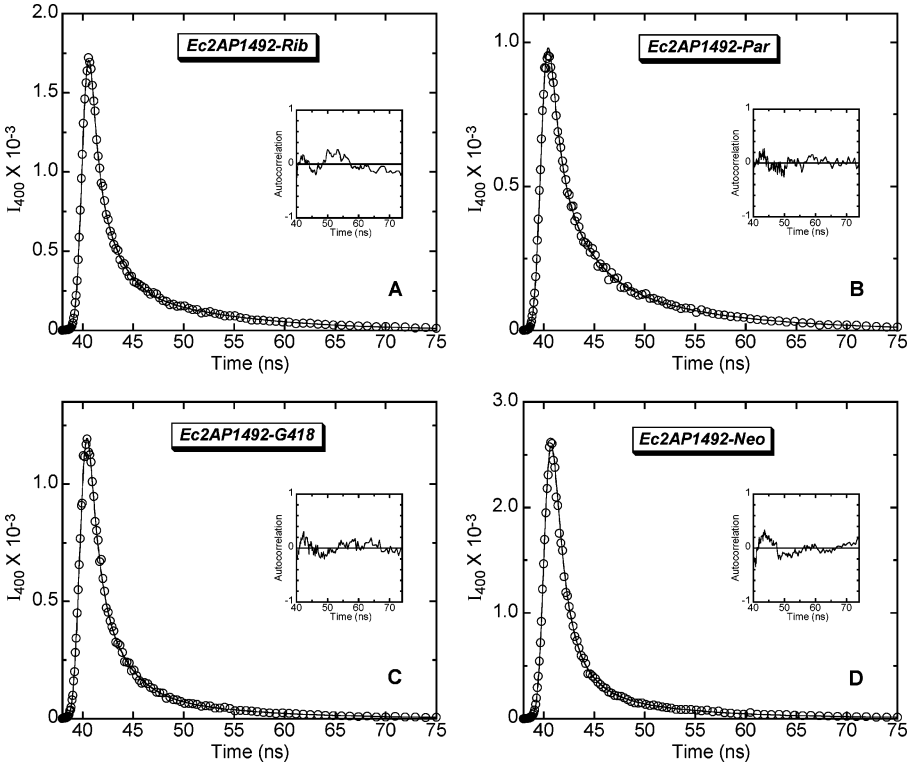

Figure 5. Time-resolved fluorescence decay profiles at 25 °C for the complexes of Ec2AP1492 with (A) ribostamycin (Rib), (B) paromomycin (Par), (C) G418, and (D) neomycin (Neo). In each panel, the open circles represent the experimental data points, while the solid lines reflect the nonlinear least-squares fits of the data with eq 1. The inset in each panel shows the autocorrelation function of the weighted residuals for the fit of the corresponding decay profile. I_{400} denotes the fluorescence emission intensity at 400 nm. Solution conditions were as described in the legend to Figure 4.

Table 3. Fluorescence Decay Parameters for Ec2AP1492 and its Complexes with Ribostamycin (Rib), Paromomycin (Par), G418, and Neomycin (Neo) at 25 °C[a]

sample	α_1	τ_1 (ns)	α_2	τ_2 (ns)	α_3	τ_3 (ns)	χ^2
Ec2AP1492	0.055 ± 0.003	9.21 ± 0.19	0.070 ± 0.002	2.85 ± 0.17	0.595 ± 0.021	0.309 ± 0.014	1.277
Ec2AP1492−Rib	0.079 ± 0.001	9.00 ± 0.08	0.283 ± 0.008	1.80 ± 0.04	0.820 ± 0.029	0.324 ± 0.019	1.863
Ec2AP1492−Par	0.043 ± 0.004	11.74 ± 0.48	0.116 ± 0.004	3.59 ± 0.22	0.294 ± 0.006	0.810 ± 0.032	1.180
Ec2AP1492-G418	0.021 ± 0.002	11.41 ± 0.48	0.171 ± 0.007	3.06 ± 0.10	0.438 ± 0.008	0.781 ± 0.034	1.210
Ec2AP1492−Neo	0.020 ± 0.003	14.47 ± 0.99	0.162 ± 0.005	4.14 ± 0.17	0.983 ± 0.007	1.017 ± 0.015	1.436

[a] For each sample, values of α_i, τ_i, and χ^2 were derived from global analyses of 10 decay curves using eq 1. The indicated uncertainties reflect the standard deviations of the experimental data from the fitted curves.

(i) In the absence of bound drug, Ec2AP1492 exhibits an $f_{stacked}$ value of 0.69. Thus, on average, the 2AP1492 residue is stacked in 69% of the Ec2AP1492 molecules. Recent crystallographic and NMR studies indicate that, in the absence of bound drug, the adenines at positions 1492 and 1493 are able to adopt both intrahelical and extrahelical conformations.[7,12,15] Together with our results, these structural observations suggest that A1492 and A1493 are in conformational equilibria between intrahelical and extrahelical states, with the intrahelical state being favored over the extrahelical state in the absence of bound drug.

(ii) The binding of each drug decreases $f_{stacked}$, an observation consistent with these drugs inducing a shift in the conformational equilibrium of the 2AP1492 residue from the intrahelical to the extrahelical state. In support of this notion, A1492 and A1493 adopt extrahelical conformations in all the NMR- and crystallographically derived structures of 2-DOS aminoglycoside−16 S rRNA A-site complexes reported to date.[5,6,8−11]

(iii) The extent to which the binding of the four drugs reduces the apparent degree of stacking of the 2AP1492 residue follows the hierarchy: paromomycin ($\Delta f_{stacked} = -0.30$) > G418 ($\Delta f_{stacked} = -0.19$) > ribostamycin ($\Delta f_{stacked} = -0.11$) > neomycin ($\Delta f_{stacked} = -0.09$). Note that this hierarchy of $\Delta f_{stacked}$ differs from the corresponding hierarchy of antibacterial activity for the four drugs (see Table 1). In particular, neomycin exhibits the most potent antibacterial activity among the four drugs, yet the RNA binding of neomycin is associated with the least negative value of $\Delta f_{stacked}$. Thus, as noted in the previous section with regard to drug affinity for the A-site, the observed extent to which drug binding reduces stacking of the 1492 base does not appear to correlate with antibacterial potency. One potential explanation for this apparent lack of correlation between observed $\Delta f_{stacked}$ and antibacterial activity is that the base at position 1492 may not be completely free of stacking interactions in its extrahelical conformation. In this connection, the bases at both positions 1492 and 1493 can adopt extrahelical conformations, and may thus engage is some degree of stacking with each other, even when in their extrahelical states. Furthermore, the extent to which these bases are stacked in their extrahelical states may differ in the different drug−RNA complexes, with larger extents of extrahelical stacking resulting in reduced magnitudes of observed $\Delta f_{stacked}$. In support of this

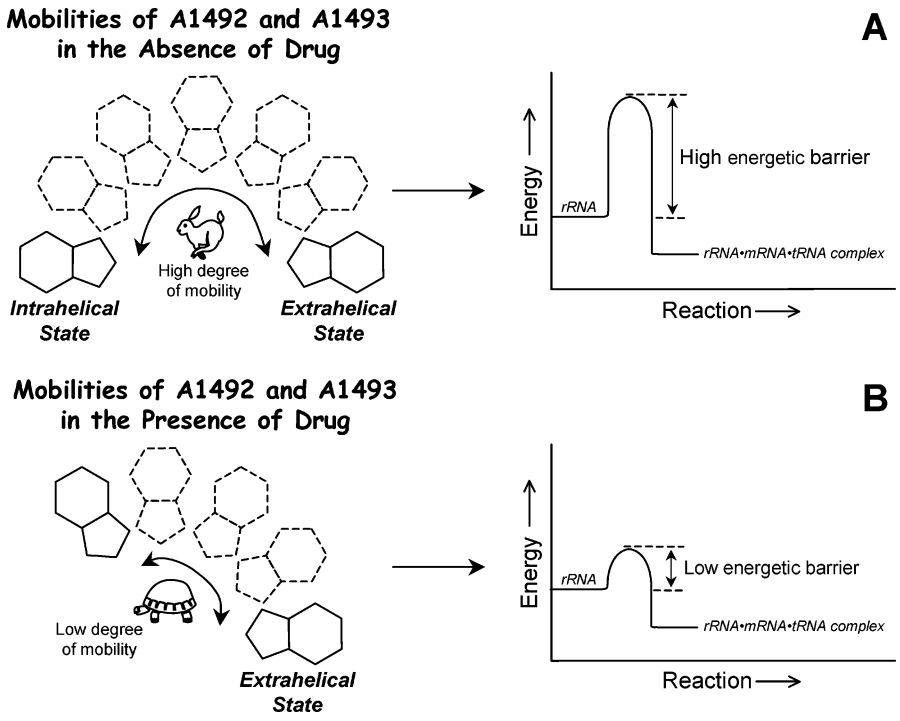

Figure 6. Schematic representations of the differential mobilities exhibited by A1492 and A1493 in the drug-free (A) and drug-bound (B) states of the 16 S rRNA, and how these differential mobilities may affect the energetics associated with the formation of the ternary rRNA·mRNA·tRNA complex. Drug binding reduces the mobilities of A1492 and A1493, which, from an entropic standpoint, should lower the energetic barrier to formation of the ternary rRNA·mRNA·tRNA complex. Note that this figure depicts only the mobilities associated with interconversion to and from the extrahelical states of A1492 and A1493. Although not depicted, the mobilities of these bases within each conformational state (e.g., mobilities related to roll and propeller twist) are also likely to influence the energetics of rRNA·mRNA·tRNA complex formation.

possibility, the crystal structures of A-site model oligonucleotides in complex with either neomycin[13] or paromomycin[9] reveal stacking interactions between the extrahelical conformations of A1492 and A1493. Significantly, the degree of stacking between the two bases is greater in the neomycin complex than in the paromomycin complex. With the reasonable assumption that 2AP residues have similar stacking properties to adenine residues (they both have a single exocyclic amino group and similar partial atomic charges), this observation is consistent with the less negative $\Delta f_{stacked}$ value we observe for neomycin (-0.09) than for paromomycin (-0.30). Thus, differences in $\Delta f_{stacked}$ may reflect not only differences in the degree to which the conformational equilibrium is shifted from the intrahelical to the extrahelical state, but also differences in the extent of stacking in the extrahelical state.

Aminoglycoside Binding Reduces the Mobility of the Base at Position 1492, with the Extent of This Reduction Correlating with Relative Antibacterial Activity. Recall that the conformational equilibria of A1492 and A1493 between their intrahelical and extrahelical states are thought to play an important role in the fidelity of translation,[14,15,17] with the mechanism underlying this role involving the interactions of these two rRNA bases with the minor groove of the minihelix formed by the tRNA anticodon and the mRNA codon (see Figure 1A). By shifting the conformational equilibria of A1492 and A1493 toward their extrahelical states, aminoglycosides enhance the interactions of A1492 and A1493 with the codon−anticodon minihelix, even in the presence of a noncognate anticodon (see Figure 1B), thereby interfering with translation.

From an entropic point of view, the interactions of A1492 and A1493 with the codon−anticodon minihelix should be influenced by the mobilities of the two rRNA bases. In this regard, high degrees of base mobility (i.e., high degrees of freedom) should disfavor the interactions by conferring a high energetic barrier to complex formation (schematically depicted in Figure 6A). By contrast, low degrees of base mobility should favor the interactions by lowering the energetic barrier (schematically depicted in Figure 6B). Thus, drugs that restrict the mobilities of A1492 and A1493 in their extrahelical states should have enhanced deleterious effects on translation and, ultimately, enhanced antibacterial potency. To evaluate the veracity of this hypothesis, we used time-resolved fluorescence anisotropy to characterize the dynamics of Ec2AP1492 in the absence and presence of the four drugs.

Figure 7 shows a representative set of polarized fluorescence intensity decays for the four drug complexes of Ec2AP1492, with the emission polarizer oriented either parallel (I_{VV}) or perpendicular (I_{VH}) to the excitation polarization. A similar set of polarized fluorescence intensity decays was obtained for drug-free Ec2AP1492 (not shown). All the polarized fluorescence intensity decays were deconvolved as described in the Materials and Methods to yield the anisotropy decay parameters listed in Table 4. The anisotropy decays were best described by the sum of two exponential terms (eq 4). The $r(0)$ values for the biexponential fits range from 0.289 to 0.373, in good agreement with previously reported $r(0)$ values for 2AP in DNA, which range from 0.266 to 0.377.[28,30,31]

(30) Nordlund, T. M.; Andersson, S.; Nilsson, L.; Rigler, R.; Gräslund, A.; McLaughlin, L. W. Structure and Dynamics of a Fluorescent DNA Oligomer Containing the *Eco*RI Recognition Sequence: Fluorescence, Molecular Dynamics, and NMR Studies. *Biochemistry* **1989**, *28*, 9095−9103.

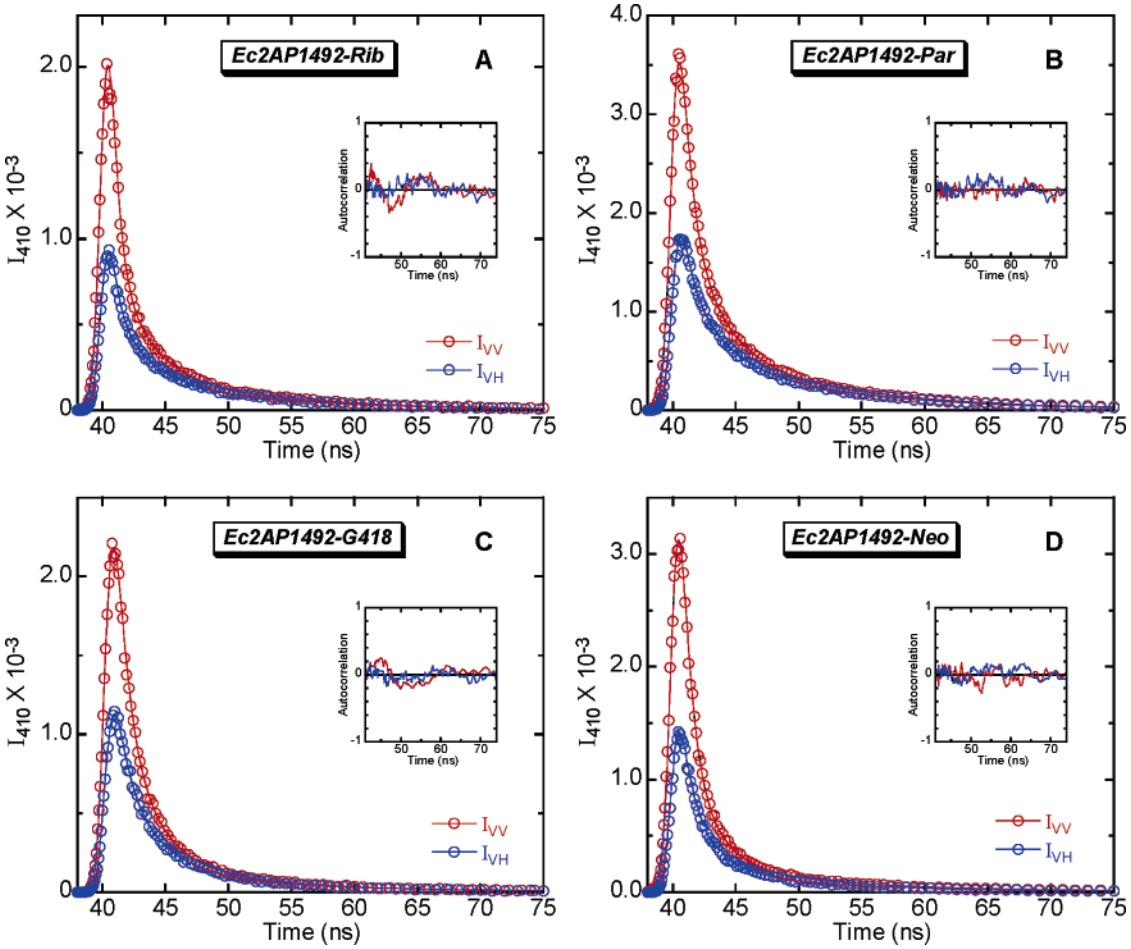

Figure 7. Polarized fluorescence intensity decay profiles at 25 °C for the complexes of Ec2AP1492 with (A) ribostamycin (Rib), (B) paromomycin (Par), (C) G418, and (D) neomycin (Neo). The decay profile with the emission polarizer oriented parallel to the excitation polarization (I_{VV}) is depicted in red, while the decay profile with the emission polarizer oriented perpendicular to the excitation polarization (I_{VH}) is depicted in blue. In each panel, the open circles represent the experimental data points, while the solid lines reflect the nonlinear least-squares fits of the data with eq 1. The inset in each panel shows the autocorrelation functions of the weighted residuals for the fits of the corresponding decay profiles. I_{410} denotes the fluorescence emission intensity at 410 nm. Solution conditions were as described in the legend to Figure 4.

Table 4. Fluorescence Anisotropy Decay Parameters for Ec2AP1492 and its Complexes with Ribostamycin (Rib), Paromomycin (Par), G418, and Neomycin (Neo) at 25 °C[a]

sample	β_1	ϕ_1 (ns)	β_2	ϕ_2 (ns)	$r(0)$[b]
Ec2AP1492	0.064 ± 0.035	7.01 ± 2.46	0.309 ± 0.025	0.54 ± 0.15	0.373 ± 0.060
Ec2AP1492−Rib	0.276 ± 0.057	5.93 ±1.48	0.045 ± 0.012	1.04 ± 0.02	0.321 ± 0.069
Ec2AP1492−Par	0.088 ± 0.033	9.69 ± 3.92	0.209 ± 0.041	1.68 ± 0.05	0.297 ± 0.074
Ec2AP1492-G418	0.160 ± 0.076	12.77 ± 3.69	0.174 ± 0.026	2.00 ± 0.10	0.334 ± 0.102
Ec2AP1492−Neo	0.026 ± 0.003	6.15 ± 1.26	0.262 ± 0.001	2.29 ± 0.07	0.289 ± 0.004

[a] For each sample, the values of β_i and ϕ_i represent averages of at least two independent experiments, with the indicated uncertainties reflecting the standard deviations from the mean. [b] Values of $r(0)$ were calculated from the sum of β_1 and β_2, with the indicated uncertainties reflecting the maximum possible errors as propagated through this summation.

The longer of the two rotational correlation times (ϕ_1) reflects the overall tumbling of the RNA duplex. In support of this assignment, we used the HYDROPRO version 5a software suite[23,24] to calculate harmonic mean rotational correlation times (ϕ_{calc}) for the NMR-derived structure of an RNA hairpin 27mer (PDB code 1a3m)[7] identical to Ec2AP1492, with the exception of having an adenine at position 1492 instead of a 2AP residue, as a function of atomic hydrodynamic radius (a). The resulting dependence of ϕ_{calc} on a is graphically depicted in Figure 8. The values of ϕ_{calc} (denoted by the filled circles in Figure 8), which ranged from 4.20 ns at an a value of 1.5 Å to 9.29 ns at an a value of 6.0 Å, were best fit by the following second-order polynomial:

$$\phi_{calc} = 0.084a^2 + 0.489a + 3.261 \quad (8)$$

Inserting our experimental ϕ_1 value of 7.01 ± 2.46 ns (denoted by the open circle in Figure 8) into eq 8 yields an a value of 4.38 Å. This a value is greater in magnitude than the 2.84 Å value that Garcia de la Torre and co-workers found to yield calculated hydrodynamic properties of several DNA oligonucleotides that were consistent with corresponding properties derived by NMR and dynamic light scattering measurements.[24] Note that the difference between the ϕ_{calc} values corresponding to a

(31) Guest, C. R.; Hochstrasser, R. A.; Sowers, L. C.; Millar, D. P. Dynamics of Mismatched Base Pairs in DNA. *Biochemistry* **1991**, *30*, 3271−3279.

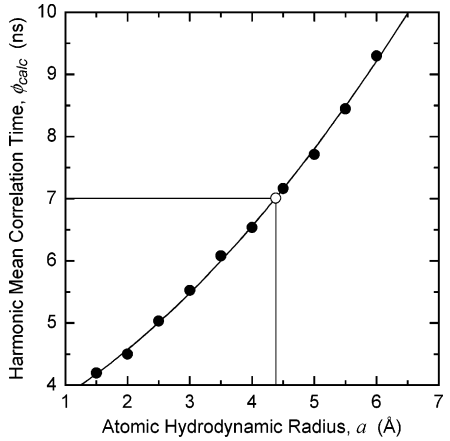

Figure 8. Dependence of the calculated harmonic mean correlation time (ϕ_{calc}) on atomic hydrodynamic radius (a). Values of ϕ_{calc} were derived as described in the Materials and Methods and are denoted by the filled circles. The curved line represents the fit of the ϕ_{calc} versus a data with eq 8. The open circle reflects the experimentally derived ϕ_1 value for Ec2AP1492 in the absence of bound drug (7.01 ± 2.46 ns), with the horizontal and vertical lines reflecting the interpolation of the a value (4.38 Å) that best fits the experimental ϕ_1 value.

values of 4.38 and 2.84 Å ($\Delta\phi_{calc}$ = 1.68 ns) is within the uncertainty (±2.46 ns) associated with our experimental value of ϕ_1. In fact, the differences between all the ϕ_{calc} values determined using a values from 2.0 to 6.0 Å and our experimental value of ϕ_1 fall within the experimental uncertainty. Viewed as a whole, the computational studies described above are consistent with ϕ_1 reflecting the overall tumbling of the RNA duplex.

The shorter rotational correlation time (ϕ_2) reflects the internal motion of the 2AP base in the RNA, with the subnanosecond value of ϕ_2 (0.54 ± 0.15 ns) obtained in the absence of bound drug being characteristic of previously reported values for 2AP residues in short DNA duplex constructs at temperatures ≥20 °C.[28,30,31] Note that drug binding increases ϕ_2, an observation indicative of a drug-induced decrease in the mobility of the 2AP base at position 1492. Furthermore, the extent to which drug binding reduces the mobility of the 2AP1492 base ($\Delta\phi_2$) follows the hierarchy: neomycin ($\Delta\phi_2$ = 1.75 ns) > G418 ($\Delta\phi_2$ = 1.46 ns) > paromomycin ($\Delta\phi_2$ = 1.14 ns) > ribostamycin ($\Delta\phi_2$ = 0.50 ns). A corresponding set of time-resolved fluorescence anisotropy characterizations of drug binding to an A-site model oligomer identical to Ec2AP1492 with the exception of having the 2AP residue at position 1493 instead of 1492 yielded a similar trend with regard to the mobility of the 2AP base at position 1493 (not shown). A comparison of the ϕ_2 data in Table 4 with the MIC data in Table 1 reveals a correlation between the relative extent of drug-induced reduction in the mobility of the base at position 1492 and relative antibacterial activity, with larger drug-induced reductions in base mobility coinciding with enhanced antibacterial potency. This observed correlation is consistent with the hypothesis noted above and schematically depicted in Figure 6. Ultimately, the generality of our observed correlation with regard to other 2-DOS aminoglycosides needs to be assessed. Nevertheless, our results highlight drug-induced alteration in the mobilities of the bases at positions 1492 and 1493 of the 16 S rRNA A-site as a potentially key determinant of antibacterial activity.

We recognize that correlating in vitro observables with biological activity can be complicated by factors that only come into play at the cellular level. One such potential factor is cellular transport. In this regard, one might suggest that the differential antibacterial activities of the aminoglycosides studied here may be dictated to a significant extent by differential transport into bacterial cells. However, a recent study by Recht and Puglisi argues against this possibility.[32] This study compared the bactericidal activities of a broad range of aminoglycosides (including those studied here) versus *E. coli* DH1 cells that differed only with respect to the sequence of their 16 S rRNA A-site, one cell type expressing wild-type 16 S rRNA and the other expressing an A1408G mutant form of the 16 S rRNA. Significantly, aminoglycosides that exhibited similar bactericidal activities versus the wild-type cells exhibited markedly differing activities versus the A1408G mutant cells. Assuming that the A1408G mutation in the 16 S rRNA does not alter transport properties, this observation suggests that the differential bactericidal activities exhibited by different aminoglycosides are not the result of differential transport.

In vitro translation assays provide a means for evaluating drug impact on protein synthesis that is not compromised by cellular transport effects. The Wong, Pelletier, and Hermann groups have conducted such assays on a structurally diverse set of aminoglycosides that includes neomycin, paromomycin, gentamicin, ribostamycin, and neamine.[33−35] Significantly, these studies show a correlation between the extent of inhibition of in vitro translation and bactericidal potency. Like the observations of Puglisi and co-workers noted above, these observations also suggest that the differential bactericidal activities among the aminoglycosides are not dictated to a significant extent by differential transport. Furthermore, in the case of neomycin, paromomycin, and ribostamycin, the extent of in vitro translation inhibition correlates with the $\Delta\phi_2$ data reported here.

Implications for the Design of Antibiotics That Target the 16 S rRNA A-Site. Structure-based drug design strategies are typically geared toward the identification and development of compounds that bind to a desired target with high affinity and specificity. Our studies suggest that high drug affinity for the A-site of 16 S rRNA is not a critical determinant of antibacterial potency. Thus, the rational design of antibiotics that target the 16 S rRNA A-site will likely require consideration of more than just structure alone. Our time-resolved fluorescence anisotropy results presented here suggest that the drug design process will also require consideration of the intermolecular and intramolecular dynamics associated with the system. In this connection, we have identified drug-induced reduction in the mobilities of the bases at positions 1492 and 1493 as a potentially key determinant of antibacterial activity. An important next step toward applying this knowledge to the drug design process will

(32) Recht, M. I.; Puglisi, J. D. Aminoglycoside Resistance with Homogeneous and Heterogeneous Populations of Antibiotic-Resistant Ribosomes. *Antimicrob. Agents Chemother.* **2001**, *45*, 2414−2419.
(33) Carriere, M.; Vijayabaskar, V.; Applefield, D.; Harvey, I.; Garneau, P.; Lorsch, J.; Lapidot, A.; Pelletier, J. Inhibition of Protein Synthesis by Aminoglycoside−Arginine Conjugates. *RNA* **2002**, *8*, 1267−1279.
(34) Greenberg, W. A.; Priestley, E. S.; Sears, P. S.; Alper, P. B.; Rosenbohm, C.; Hendrix, M.; Hung, S.-C.; Wong, C.-H. Design and Synthesis of New Aminoglycoside Antibiotics Containing Neamine as an Optimal Core Structure: Correlation of Antibiotic Activity with in vitro Inhibition of Translation. *J. Am. Chem. Soc.* **1999**, *121*, 6527−6541.
(35) Zhou, Y.; Gregor, V. E.; Sun, Z.; Ayida, B. K.; Winters, G. C.; Murphy, D.; Simonsen, K. B.; Vourloumis, D.; Fish, S.; Froelich, J. M.; Wall, D.; Hermann, T. Structure-Guided Discovery of Novel Aminoglycoside Mimetics as Antibacterial Translation Inhibitors. *Antimicrob. Agents Chemother.* **2005**, *49*, 4942−4949.

be to delineate the specific molecular forces that govern the mobilities of A1492 and A1493 in both the presence and absence of drug.

Acknowledgment. We thank Dr. Smita S. Patel for use of her PTI LaserStrobe fluorescence lifetime spectrometer. This work was supported by NIH Grant CA097123. M.K. was supported by an NIH postdoctoral fellowship (F32 AI62041). C.M.B. was supported by an NIH training grant (5T32 GM08319) in Molecular Biophysics.

JA056159Z